Emulsification using a “Sonolator” liquid whistle: A new correlation for droplet size from pilot-scale experiments

Ryan, David J.; Simmons, Mark J.h.; Baker, Michael R.; Kowalski, Adam J.

DOI:
10.1016/j.ces.2018.06.004

Chemical Engineering Science 189 (2018) 369–379

Contents lists available at ScienceDirect

Chemical Engineering Science

journal homepage: www.elsevier.com/locate/ces

Emulsification using a "Sonolator" liquid whistle: A new correlation for droplet size from pilot-scale experiments

David J. Ryan [a], Michael R. Baker [b], Adam J. Kowalski [b], Mark J.H. Simmons [a,*]

[a] School of Chemical Engineering, University of Birmingham, Edgbaston, Birmingham B15 2TT, UK
[b] Unilever Research & Development, Port Sunlight Laboratory, Quarry Road East, Bebington, Wirral CH63 3JW, UK

HIGHLIGHTS

- Emulsion drop sizes measured on a pilot – scale liquid whistle device.
- Three orders of magnitude of dispersed phase viscosity considered.
- Drop size scales with pressure drop, drop viscosity and surfactant concentration.
- Expected regime change from turbulent inertial to turbulent viscous not observed.

ARTICLE INFO

Article history:
Received 12 February 2018
Received in revised form 15 May 2018
Accepted 1 June 2018
Available online 2 June 2018

Keywords:
Sonolator
Liquid whistle
Turbulence
Emulsification
Orifice

ABSTRACT

Emulsification experiments have been carried out on a pilot-scale Model ACIP2 Sonolator liquid whistle device by examining the change in droplet size distributions of silicone oil in water emulsions, using SLES as a surfactant, before and after processing. The process variables considered were mass flow rate, pressure drop across Sonolator, oil viscosity (from 10 to 10,000 cSt), oil concentration (0.5–10 wt%), surfactant concentration (0.00003–0.5 wt%) and orifice size. All experiments were carried out in the turbulent flow regime. The oil phase was added as either a pure phase or as a pre-emulsion stabilised using SLES. The oil was injected just before the blade or mixed at a T-junction prior to the Sonolator; the pre-emulsion was exclusively introduced via the latter method. The resultant droplet size distributions were obtained from offline sampling using laser diffraction. The most significant parameters found to influence the drop size were found to be pressure drop, dispersed phase viscosity and surfactant (SLES) concentration, which formed the basis for an empirical power law correlation. Indices in this correlation were compared to findings in the literature for other emulsification devices, and to those predicted from the theories of droplet breakage in turbulent inertial flow. Despite an expected regime change from turbulent inertial to turbulent viscous break-up being common in the literature as the dispersed phase viscosity is increased, this phenomenon was not observed in the experimental data obtained, suggesting breakage in an intermediate regime.

1. Introduction

The Sonolator (ex. Sonic Corp, USA) is an inline fluids processing device of the liquid whistle type which causes mixing and emulsification of multiphase fluids resulting in finely dispersed droplets. To enable the integration of such a device into a process line, it is necessary to understand how the process parameters are correlated with the reduction in droplet size, with critical parameters including the mass flow rate of fluid and the size of the orifice. Such information is necessary for industrial research and development enabling minimization of costly and lengthy pilot scale experimentation. New products or necessary modifications could then be applied to existing plant with confidence *a priori*, with the ultimate gain of reduction of time to market for new products and their associated processes.

The theoretical treatment of droplet breakage under the action of fluid flow stems from the principle that a droplet in a flow remains stable provided that the internal cohesive forces (due to viscosity and interfacial tension) are greater than the external deformation stresses; if the opposite is true then breakage occurs. In turbulent flows, which are relevant to the Sonolator used in this study, the external forces are driven by the turbulent eddies within the flow; the smallest of these can be estimated using the Kolmogorov length scale, l_e and time scale, t_e

* Corresponding author.
E-mail address: m.j.simmons@bham.ac.uk (M.J.H. Simmons).

https://doi.org/10.1016/j.ces.2018.06.004
0009-2509/

Nomenclature

Symbol

A_o	area of Sonolator orifice (m^2)
a_s	specific surface area (m^{-1}, or $m^2 \cdot m^{-3}$)
C	numerical constant in a correlation
d	general droplet size (m)
$d(k)$	diameter of the kth percentile droplet in the volume-weighted DSD (m)
d_{32}	volume-surface (Sauter) mean diameter (m)
d_{43}	volume-weighted mean diameter (m)
d_{max}	maximum stable droplet size in turbulent flow (m)
d_{nm}	generalized moment-moment mean diameter (m)
$f(x)$	the number weighted droplet size distribution
l	length scale intermediate between Kolmogorov micro-scale and flow geometry (m)
l_e	Kolmogorov eddy length microscale (m)
L	characteristic length scale (m)
M	mass flow rate ($kg \cdot s^{-1}$)
N	angular velocity in stirred tank experiments in literature (rpm)
P	power dissipated in Sonolator (W)
ΔP	pressure drop across Sonolator (Pa)
Q	volumetric flow rate ($m^3 \cdot s^{-1}$)
s	logarithmic skewness of a droplet size distribution
t_e	Kolmogorov eddy time microscale (s)
U	characteristic velocity (for Re)
V'	"V prime" – size of average velocity fluctuation ($m\ s^{-1}$)
w_{SLES}	concentration of SLES (w/w)
w	logarithmic span of a droplet size distribution
x	variable on horizontal axis of graph
y	variable on vertical axis of graph

Units

cSt	centistokes, unit of kinematic viscosity; equivalent to $10^{-6}\ m^2\ s^{-1}$

Subscripts

c	continuous phase (water)
d	discrete phase (oil)
def	deformation
e	eddy
max	maximum (droplet size)

Greek symbols

β	beta, constant relating effect of viscosity to interfacial tension
ε	epsilon, local specific turbulent energy dissipation rate ($m^2 \cdot s^{-3}$ or $W \cdot kg^{-1}$)
ν_c	kinematic viscosity of continuous phase ($m^2 \cdot s^{-1}$)
ν_d	nu, kinematic viscosity of dispersed phase ($m^2\ s^{-1}$)
μ_d	mu, dynamic viscosity of dispersed phase (Pa s)
ρ	rho, density of fluid ($kg\ m^{-3}$)
σ	sigma, interfacial tension ($N\ m^{-1}$)

Dimensionless groups

φ	dispersed phase volume fraction
C_D	discharge coefficient of Sonolator orifice
R^2	coefficient of determination, close to unity when scatter is close to zero.
Re	Reynolds number
We	Weber number

Abbreviations

CMC	critical micelle concentration (of a surfactant)
DSD	droplet size distribution
INJ	oil inlet condition of being injected at the orifice
PE	oil inlet condition of aqueous pre-emulsion with 0.5 wt % SLES
SLES	sodium laureth sulphate, or sodium lauryl ether sulphate
TI	turbulent inertial droplet breakage regime
TMIX	oil inlet condition of mixing at a T-junction
TV	turbulent viscous droplet breakage regime

$$l_e = \left(\frac{\nu_C^3}{\varepsilon}\right)^{1/4}, \tag{1}$$

$$t_e = \left(\frac{\nu_C}{\varepsilon}\right)^{1/2}, \tag{2}$$

where ε is the power input per unit mass of fluid and ν_C is the continuous phase kinematic viscosity. The largest turbulent eddies are at length scales (L) comparable with the flow geometry and $l_e \ll L$. Regarding external forces, if $l_e \ll d \ll L$ for a breaking droplet of diameter, d, then the droplet tends to be broken apart by pressure fluctuations from multiple turbulent eddies surrounding the droplet. This case is the turbulent inertial (TI) regime. Alternatively, if the droplet is smaller than l_e (e.g. $d \ll l_e$) then only viscous shear, if sufficient, can disrupt the droplet: this turbulent viscous (TV) regime has been observed in very high shear devices such as small-gap homogenisers. For low-viscosity dispersed phases, the cohesive force comes from interfacial tension whilst for high-viscosity dispersed phases, the cohesive force comes from the viscous force opposing deformation. These two regimes (low/high viscosity) can also be separated out by considering the deformation time compared to the characteristic time of the surrounding turbulent eddy or eddies. For further discussion see Walstra and Smulders (1998), Padron (2005) and Hall (2012).

In the Sonolator after the orifice (where droplet breakage is believed to occur) the Reynolds number is in the turbulent range, with typical values between 7000 and 150,000 at the orifice. Moreover, the droplet sizes are initially much larger than the associated Kolmogorov microscale, and remain so throughout emulsification. Hence breakage occurs fully within the turbulent inertial (TI) regimes. Many droplet size correlations have been developed to predict droplet size on the basis of existing emulsification experimental data, with TI experiments being easier to carry out than TV experiments, since the final droplet size is larger and requires less energy to access. Hinze (1955) gave the well-known result for prediction of maximum stable droplet size, d_{max} in inviscid TI droplet breakage assuming local isotropy and a dilute dispersed phase,

$$d_{max} = C \cdot \varepsilon^{-2/5} \rho_c^{-3/5} \sigma^{3/5} \tag{3}$$

where σ is the interfacial tension, ρ_c is the continuous phase density, and the constant, $C = 0.725$ (i.e. of order of unity). For apparatus where ε is proportional to flow rate cubed (e.g. the Sonolator) the dependence of d_{max} upon flow rate (mass or volumetric) would therefore be a power law of index −1.2.

Davies (1985, 1987) modified Hinze's expression to incorporate the effects of dispersed phase viscosity. During turbulent droplet breakage, as the dispersed phase viscosity increases, the dominant

droplet cohesive force changes from interfacial tension driven to a viscous resistance to deformation. Davies included this effect by modifying the critical Weber number during breakage to have two terms, one for interfacial tension (σ) and an extra term for dispersed phase viscosity (μ_D) scaled by a constant determined from experiment (β) and the size of local velocity fluctuations (V'), giving:

$$d_{max} = C \cdot \varepsilon^{-2/5} \rho_c^{-3/5} (\sigma + \beta \mu_D V')^{3/5} \quad (4)$$

For high μ_D, (4) may be simplified by removal of the σ term. In addition, the fluctuating velocity V' can be modelled by $(\varepsilon\, d_{max})^{1/3}$ in homogeneous turbulent flow. Combining these, a result equivalent to that obtained by Walstra and Smulders (1998) is obtained, i.e.

$$d_{max} = C \cdot \varepsilon^{-1/4} \rho_c^{-3/4} \mu_D^{3/4} \quad (5)$$

Thus, droplet size is expected to scale with $\varepsilon^{-0.25}$, which in the Sonolator is flow rate to the power −0.75. Hence, (3) from Hinze (1955) is suitable for predicting droplet size in low-viscosity TI breakage, (5) from Walstra and Smulders (1998) is suitable for predicting droplet size in high-viscosity TI breakage, and (4) from Davies (1985, 1987) gives a prediction of what should happen between these two regimes.

In (3) and (5) dispersed phase viscosity (μ_D) has index 0 and 0.75 respectively. Both (3) and (5) are limit cases of (4), hence equation (4) suggests that the slope of a graph of d_{max} versus dispersed phase viscosity (μ_D), for fixed ε, should have zero slope at low viscosity and a slope of 0.75 at high viscosity, with a smooth interpolation between these two extreme cases.

Although large number of works have applied these principles to examine emulsification within stirred vessels over wide ranges of viscosity ratio and process conditions e.g. Chen and Middleman (1967), Arai et al. (1977), Calabrese et al. (1986), Wang and Calabrese (1986), works published on continuous flow systems such as the Sonolator are comparatively few. Davies (1987) attempted to correlate a wide variety of emulsification devices via a plot of Sauter mean diameter, d_{32} vs ε including static mixers, agitated vessels, colloid mills, liquid whistles and valve homogenizers. The data points fell between two parallel lines of slope −0.4; this validated (3) for low viscosity TI and demonstrated that the constant in this equation thus had quite a narrow range across a large number of devices.

Of the limited number of studies in continuous devices, Ludwig et al. (1997) considered formation of emulsions in a screw loop reactor, finding the slope of d_{max} vs ε equal to −0.4 on a log-log plot, and similar patterns to Arai et al. (1977) were found for the d_{max} vs oil viscosity plot: flat for low viscosity, sharp gradient around 100 cSt, levelling off at higher viscosities. This shows that the droplet breakage mechanisms in turbulent inertial flow are independent of the exact device used. However in high pressure homogenizers (HPH) quoted indices of dependence include: 0.7 (Pandolfe, 1981), 0.4 (Karbstein, 1994) and 0.33 (Walstra and Smulders, 1998), so there is a considerable discrepancy here. HPH are similar to the Sonolator in that emulsification in both devices is carried out by forcing a multiphase liquid through a small opening.

Hall et al. (2011, 2013) considered existing results concerning batch and in-line rotor-stator devices: for batch devices Francis (1999) and Calabrese et al. (2000) correlated droplet size with Weber number to the power −0.58, very close to the low-viscosity TI theoretical value of −0.6. Puel and Briancon (2006) also obtained a Weber number index of −0.6; for in-line devices Koglin et al. (1981) obtained droplet size correlation with $\varepsilon^{-0.4}$; other breakage regimes were also covered.

In summary, there is good experimental evidence to support (3) for low viscosity droplet breakage in the turbulent inertial (TI) regime, and also (5) for higher viscosity breakage in continuous systems. (4) is supported in a limited range but with some evidence of a variation in slope for very high dispersed phase viscosities, and some variation in reported viscosity index for high pressure homogenizers.

No data for droplet break up for a Sonolator device exist in the open literature, although Ryan et al. (2017) report the first full attempt to measure and model the flow fields within a pilot-scale Sonolator "Model A" device using particle image velocimetry and computational fluid dynamics respectively. However emulsification has been characterised for many other fluid mixing devices, most recent examples include ultrasonic emulsification (Lin and Chen, 2006); six vaned rheometer (Baravian et al., 2007); narrow gap homogenizers (Vankova et al., 2007); valve homogenizers or HPH (Tesch et al., 2003); batch rotor stator devices (Calabrese et al., 2000; Padron, 2005) and inline rotor stator devices (Hall et al., 2011, 2013). All of these generate turbulence which, depending on the exact flow conditions, may break droplets in a similar way to the Sonolator. The emulsions produced in the above studies were mostly oil in water (O/W), with the dispersed oil phase generally being of higher viscosity unless thickening agents were introduced into the aqueous phase (e.g. Hall et al., 2011). Dispersed phases investigated include silicone oils of varying viscosity (Padron, 2005, Hall et al., 2011, 2013), which possess the advantage that their viscosity can be varied over at least three orders of magnitude without affecting other physical properties. Various surfactants have been employed, with low molecular weight surfactants such as Span 80 (Lin and Chen, 2006), Tween 60/80 (Tesch et al., 2003; Lin and Chen, 2006), SDS (Tesch et al., 2003; Vankova et al., 2007) and sodium lauryl ether sulphate (SLES) (Hall et al., 2011) having the advantage that they migrate to the newly formed droplet interfaces faster than high molecular weight surfactants, minimizing opportunity for re-coalescence. Two methods of measuring drop size have been employed, either optical/video microscopy or laser diffraction, the latter being much more rapid compared to manual sizing of particles. For example, Hall et al. (2011, 2013) used laser forward scatter to obtain drop size using a Malvern Mastersizer 2000 from samples taken from an inline Silverson rotor-stator device.

The work presented in this paper utilises the same silicone oil dispersed in water (in the presence of SLES) emulsification system from the study by Hall et al. (2011, 2013), which is applied to a pilot-scale Model ACIP2 Sonolator. The effect of process parameters (mass flow rate, pressure drop, oil viscosity, oil concentration, surfactant concentration, oil inlet condition and orifice size) upon the average drop size produced are examined. The drop size distributions were obtained by offline measurements using laser diffraction. This paper ascertains which of the variables have a significant effect on droplet size and an empirical correlation is developed which is compared with theoretical predictions for relevant breakage regimes.

2. Materials and methods

2.1. Materials

The physical properties of materials used are given in Table 1. Measurements of refractive index were carried out on a RFM340 automatic digital refractometer (Bellingham Stanley Ltd., UK) at Unilever Port Sunlight R&D. The density measurements were carried out using a density cup.

The water used was demineralised mains water. The surfactant used was 1EO grade SLES Texapon N701, Cognis UK Ltd, UK. The

Table 1
Material properties under ambient conditions. References: (a) author's measurement, (b) Hall, 2012, (c) Hall et al., 2011, (d) manufacturer quoted figures (e) Padron, 2005.

Material	Density ($kg \cdot m^{-3}$)	Kinematic viscosity (cSt)	Surface tension ($mN \cdot m^{-1}$)	Interfacial tension with 0.5 wt% SLES solution ($mN \cdot m^{-1}$)	Refractive index
Water	997[a]	0.89	72.0[e]	NA	1.333[a]
DC245	952[a]	3.8[d]	Unknown	Unknown	1.397[a]
Silicone oil (10 cSt)	937[c]	10[d]	20.1[b]	10.6[c]	1.399[b]
Silicone oil (350 cSt)	969[c]	350[d]	21.1[b]	12.3[c]	1.403[b]
Silicone oil (10,000 cSt)	970[b]	10,000[d]	21.5[b]	Unknown	1.404[b]
SLES solution (0.5 wt%)	998[b]	0.90[b]	Unknown	NA	1.334[a]

SLES had a molecular weight of approximately 420 $kg \cdot kmol^{-1}$, density of 1030 $kg\,m^{-3}$ and a CMC in water of 0.2 $mol\,m^{-3}$ (El–Hamouz, 2007). Calculations from this data showed that the CMC (critical micelle concentration) of SLES was around 0.0081 wt% with an air interface. Assuming that with an oil interface the CMC was of approximately equal magnitude, for 0.5 wt% emulsions used in this work, SLES was present at around 60 times the CMC. Due to this excess of surfactant, droplets would quickly become coated with SLES and become stabilised against coalescence, with full surface coverage expected. Moreover, since SLES is a small molecule fast movement from bulk to surface is expected giving negligible effects due to dynamic interfacial tension (Hall et al., 2011).

The silicone oils used were poly-dimethyl siloxane Dow Corning 200 fluids (viscosities in cSt: 10, 350, 10,000) and DC245 fluid (viscosity 3.8 cSt). These materials differed greatly in their viscosities, but other relevant material properties such as interfacial tension with water, density and refractive index were comparable. The liquids were assumed as Newtonian though there is some evidence of shear-thinning behaviour in oils with viscosities exceeding O (1000 cSt), especially at high shear rates.

2.2. Model ACIP2 Sonolator device and experimental rig

Model ACIP2 Sonolators (ex. Sonic Corporation, CT, USA) with orifice size codes 0025, 0060, 0080 and 0140 were used in pilot plant studies. The Sonolator rigs used were located at Unilever Research & Development, Port Sunlight, UK. A schematic of the Sonolator device is given in Fig. 1a, consisting of: inlet (on left), orifice, main chamber and blade (middle), outlet (right). Each component shown is cylindrical, except the blade which is shown in cross-section. The main chamber had diameter of 25.4 mm. The blade was positioned 4 mm after the orifice and the fluid flowed above and below the blade.

A photograph of a typical Sonolator orifice is given in Fig. 1b. All orifices were shaped like a "cats-eye" with an approximate perimeter of two semi-circles. Each orifice was created by milling two cuts at 60° into a hollow steel cone. The intersection of the cavity and the cuts created the orifice.

A schematic of the experimental setup used for the Sonolator runs is given in Fig. 2. The main components were aqueous phase (150 L) and oil phase (70 L) vessels, pumps with flow meters, pipe-work of 12.5 mm diameter combining the two streams at a

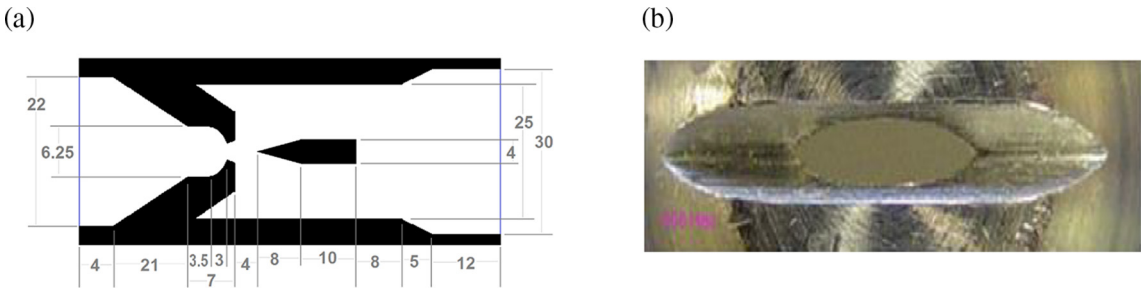

Fig. 1. (a) Schematic diagram of cross-section through thin axis of orifice, of flow domain inside ACIP2 Sonolator. All dimensions converted to millimetres from original design drawing in inches. Reproduced with corrections from Ryan (2015); (b) Photograph of pilot plant Sonolator orifice 0060.

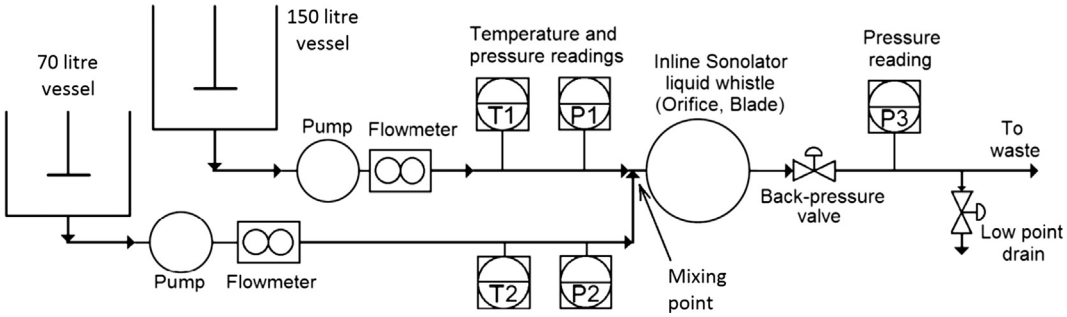

Fig. 2. Schematic diagram of Sonolator experimental setup.

T-junction or injector, the Model ACIP2 Sonolator with backpressure valve and a waste stream with a sampling point. The backpressure valve was a movable conical restriction in the cylindrical outlet pipe, and was used to maintain the pressure in the main chamber to control cavitation. The pumps used were either progressive cavity pumps (Seepex) or triplex plunger pumps (Cat) depending on the viscosity of the fluid being pumped. All flow meters were calibrated against timed flows, e.g. by weight of material collected over a set period.

The 150 L tank contained the 0.5 wt% aqueous SLES solution. Three types of process denoted PE, TMIX, INJ were run. For the PE process, the 70 L tank was filled with either a 5 wt% or 10 wt% coarse pre-emulsion of oil in water, stabilised by 0.5 wt% SLES; for TMIX and INJ processes the 70 L tank contained pure oil. For the INJ process the oil was injected just before the blade using an injector; for PE and TMIX processes the output of the 70 L tank was mixed at a T-junction prior to the Sonolator.

The effect of varying SLES concentration was investigated using the TMIX set up. This was achieved by making the aqueous phase vessel contain water only, and adding a third tank and stream with a low percentage of SLES (1.25 wt% in one experiment, 0.03125 wt % in another). By combining streams of pure oil, pure water and SLES solution, emulsification was carried out varying both flow rates and SLES concentration simultaneously over wide ranges.

Samples were taken from the low point drain of the device (Fig. 2), their stability was ensured by sampling into 1 wt% SLES solution at a ratio of approximately 1:1 between the SLES solution and the emulsion sample; this prevented coalescence from altering the droplet size distribution after sampling.

2.3. Experimental conditions, procedure and analysis

The parameters which required specification during the Sonolator pilot plant runs were as follows: mass flow rate (obtained by adjusting set points on the mass flow controllers), orifice size, oil viscosity, oil concentration, surfactant concentration and backpressure valve position. The experimental rig setup was varied between pre-emulsion, mixing at a T-junction and injection. The experimental conditions set are given in Table 2, covering 175 data points during 10 sets of trials. Note: orifice size code "0060" meant a manufacturer stated nominal area of 0.0060 in^2 (3.87 mm^2), and similarly for other size codes. With the apparatus limitations in mind (e.g. fixed orifice sizes and limited oil viscosities available) as wide a set of flow conditions as possible were chosen.

Before each run the tanks and pipes were cleaned with hot water and surfactant solution to eliminate any build-up from previous experiments. The tanks were then charged with the raw materials. To make the aqueous SLES solutions, a 28% by mass solution of SLES was diluted to the required concentration in the 150 L tank (Fig. 2) using an impeller to circulate and mix the fluid; Hall (2012) stated that ten minutes was sufficient to completely dissolve and mix the solution.

For each flow condition set, the rig was allowed to equilibrate for at least 2 min to allow pressure drop and flow rates to stabilise. Samples were taken from the low-point drain directly after the Sonolator; the emulsion took less than thirty seconds under all flow rates to travel from the Sonolator to the low point drain.

A Malvern Mastersizer 2000 (Malvern Instruments, Malvern, UK) with a Hydro SM small volume dispersion unit was used to characterise the samples. For each sample, the cuvette was first cleaned with SLES solution to eliminate any residues; it was found not necessary to repeat this later on as long as the dispersant contained SLES. The dispersant in the Hydro SM was dilute SLES solution (0.1 wt% to 0.5 wt%) which prevented oil droplets from depositing on the cuvette and the tubing of the Mastersizer. Care was taken to eliminate air bubbles by ensuring the impeller in the Hydro SM dispersant unit was set not too high to discourage foaming, <1300 rpm. At least two separate measurements were carried out on each sample. Previous tests by Hall (2012) showed that the presence of air bubbles was easily detectable due to their larger size and random occurrence in the data – no such issues were observed in this data which followed the same experimental protocol.

3. Theory

The Reynolds number (Re) can be defined as

$$Re = \frac{U \cdot L}{\nu_C}, \tag{6}$$

where U is the characteristic velocity, L is the characteristic length scale (L) and ν_c is the kinematic viscosity of the fluid (continuous phase). The Reynolds number was calculated both at the restriction

Table 2
Descriptions of Sonolator experimental runs.

Trial-set number	Orifice size (in^2, mm^2)	Orifice size code	Oil inlet condition	Oil viscosities (cSt)	Back pressure valve	Mass flow rate setpoints ($kg \cdot s^{-1}$)	Oil weight fractions	SLES weight fractions
1	0.0060 3.87	0060	PE	10	Closed	0.033–0.100	Below 10%	0.5 wt%
2	0.0060 3.87	0060	PE	10	Open	0.033–0.215	Below 10%	0.5 wt%
3	0.0060 3.87	0060	PE	350	Open	0.033–0.218	Below 10%	0.5 wt%
4	0.0080 5.16	0080	PE	350	Open	0.067–0.283	Below 10%	0.5 wt%
5	0.0140 9.03	0140	PE	350	Closed	0.150–0.333	Below 10%	0.5 wt%
6	0.0140 9.03	0140	PE	350	Open	0.150–0.333	Below 10%	0.5 wt%
7	0.0025 1.61	0025	PE	10, 350	Open	0.033–0.100	0.5–10 wt%	0.5 wt%
8	0.0025 1.61	0025	PE	3.8, 350, 10 000	Open	0.008–0.108	0.5–5 wt%	0.5 wt%
9	0.0080 5.16	0080	INJ, TMIX	10, 350	Open	0.118–0.288	2 wt%, 5 wt%	0.5 wt%
10	0.0080 5.16	0080	TMIX	3.8, 350	Open	0.073–0.288	2 wt%, 5 wt%	0.5–0.0003 wt%

Table 3
Reynolds number statistics summarizing 175 different pilot plant experiments. Average and standard deviation (SD) calculated using logarithms of original data.

	Minimum	Average – SD	Average	Average + SD	Maximum
Orifice	7403	37,815	68,325	123,451	143,206
Main Chamber	471	3336	6856	14,091	18,853

caused by the narrow orifice and in the cylindrical main chamber (see Table 3).

At the orifice the characteristic velocity and length scales were calculated from orifice superficial velocity and square root of orifice area respectively; the Reynolds numbers were all above 7000 and consistent with fully turbulent flow for $Re > 2300$ (assuming pipe flow). Since all fluid traverses the orifice, all emulsified fluid encounters turbulent conditions. In the main chamber the characteristic velocity and length scales came from the superficial velocity and the main chamber diameter; the majority of Reynolds numbers were above 3336 and thus also turbulent.

Values of the Kolmogorov length scale (l_e) at the orifice were calculated directly using (1). Values of local specific turbulent energy dissipation rate, ε, were obtained from our previous paper where they were calculated from the fluctuating velocity gradients measured using PIV. In the orifice region, these values were found to be in good agreement with CFD predictions (see Ryan et al., 2017). Thus, the Kolmogorov eddy length scale at the orifice was calculated for 175 pilot plant experiments; comparative values of d_{32} values from each experiment are between 2.2 and 13.9 times larger (Table 4). Therefore the emulsification regime may be assumed as Turbulent Inertial (TI), in the following analysis.

4. Results and discussion

4.1. Drop size distributions

The Sauter mean diameter (d_{32}) was the key statistic examined alongside the drop size distributions (DSDs), since the emulsion properties of interest to industry often depend upon the interfacial area exposed by the droplets, which is directly related to d_{32}. DSDs of the coarse pre-emulsions are shown in Fig. 3. The DSDs for the two low viscosity oils (DC245, 10 cSt silicone oil) were log-normal, with the variation in peak droplet size being due to different rates of stirring in the oil phase tank. The higher viscosity 350 cSt and 10,000 cSt oils had a larger spread of droplet sizes in the pre-emulsion and their distributions were negatively skewed. Fig. 3 also shows the processed samples for both the 10 cSt and 350 cSt oils where in all cases there was a reduction of droplet size after the fluids were processed, this was seen by the distribution shifting towards the left by close to an order of magnitude in all cases; this clearly shows the impact of emulsification in the Sonolator. Moreover, the distributions obtained at 0.100 kg·s^{-1} were shifted further to the left than the corresponding 0.033 kg·s^{-1} distributions, which indicated a further reduction in droplet sizes when processing with higher flow rates. Hall et al. (2011), who used an identical preparation protocol for the silicone oil in water emulsions used here, show that the outlet drop size from an inline high shear rotor-stator mixer is insensitive to the inlet droplet size distribution of the coarse pre-emulsion used; the drop size decrease is an order of magnitude or more in their experiments.

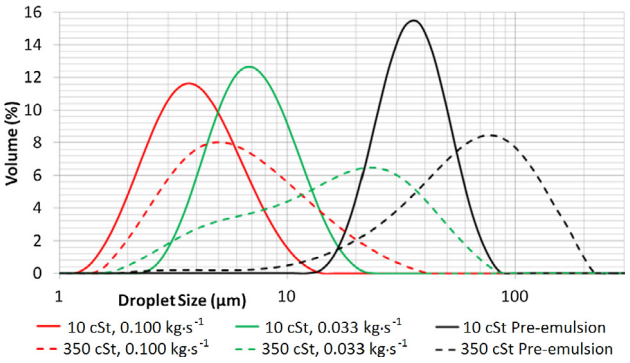

Fig. 3. Volume weighted DSDs for 10 cSt and 350 cSt oil. Comparison between: pre-emulsion, processing at 0.033 kg s^{-1}, processing at 0.100 kg s^{-1} for 0025 orifice.

Given the similar findings in this study, we would expect a similar insensitivity to inlet drop size, though this was not explicitly investigated.

The effect of oil viscosity and flow rate are shown more clearly in Fig. 4 where pre-emulsions of silicone oils with four different viscosities (3.8, 10, 350, 10,000 cSt) were processed on the Sonolator with a 0025 orifice. Fig. 4a shows that for the 3.8 cSt oil the distributions were log-normal, as would be expected for successive break up of droplets, see for example Marmottant and Villermaux (2004), with slightly narrower distributions for the middle flow rate of 0.067 kg·s^{-1} (in green), with a single peak droplet size which decreased with increasing mass flow rate. This dependency was expected since energy dissipation rate scales according to the cube of mass flow rate, in line with existing theories e.g. Hinze (1955). Similar results are found for the 10 cSt silicone oil in Fig. 4b.

Fig. 4c also shows that for 350 cSt oil as flow rate increased the droplet sizes decreased. This time however the distributions were not log-normal, indeed neither was the pre-emulsion DSD. Instead of the peak droplet size shifting smoothly towards the left (i.e. modal droplet size reducing) as flow rate increased, now the distributions appeared to skew towards the left with the right hand peak reducing in size and the left hand peak increasing in size, with no pronounced intermediate size peak for intermediate flow rates. This caused the distributions to be negatively skewed for low flow rates (large droplets) and positively skewed for high flow rates (small droplets). This is an indication that there may be a transition to a different droplet breakage mechanism as the viscosity of the oil is increased from 10 cSt to 350 cSt.

Fig. 4d shows results for the 10,000 cSt oil. Although there is a droplet size reduction as mass flow rate is increased, the distributions are now bimodal. The main impact of increasing mass flow rate was to reduce the peak on the right hand side for large droplets and to increase a peak on the left hand side for small droplets.

Table 4
Kolmogorov length scale (l_e) statistics summarizing 175 different pilot plant experiments. Average and standard deviation (SD) calculated using logarithms of original data.

Statistic	Minimum	Average – SD	Average	Average + SD	Maximum
Kolmogorov Length Scale (l_e, μm)	0.76	1.02	1.55	2.36	5.22
d_{32}/l_e	2.2	3.3	4.7	6.6	13.9

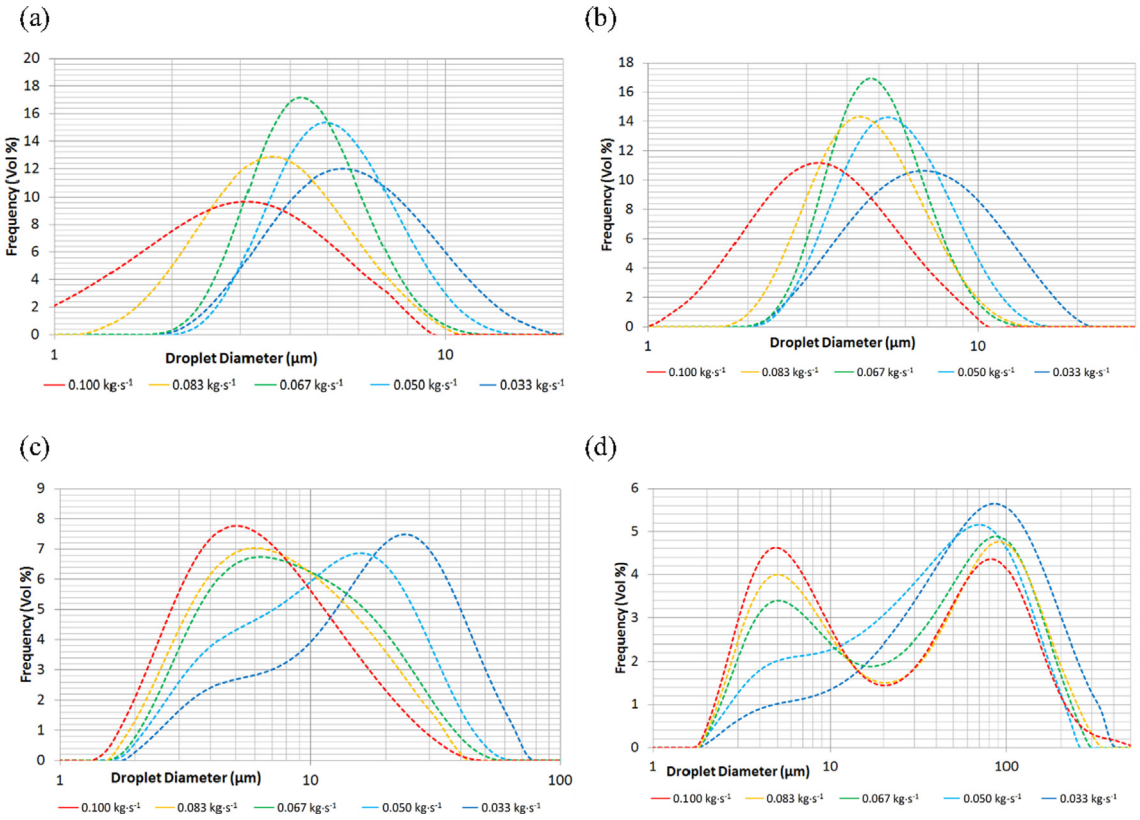

Fig. 4. Droplet size distributions for pre-emulsion (PE) setup, 0025 orifice size code, mass flow rates evenly spaced from 0.100 kg s^{-1} (red, on left) down to 0.033 kg s^{-1} (blue, on right), silicone oil pre-emulsions of viscosities: (a) 3.8 cSt (DC245); (b) 10 cSt; (c) 350 cSt; 10,000 cSt.

This could indicate a very different droplet break-up mechanism from oils of viscosity 10 cSt and below, and that possibly 350 cSt oil had a break-up mechanism intermediate between 10 cSt and 10,000 cSt cases. The theoretical correlations (3) and (5) are for low-viscosity TI breakage and high-viscosity TI breakage regimes respectively; the different break-up mechanism could be as a result of going from the former breakage regime to the latter.

A comparison of calculated Sauter mean diameters, d_{32}, from the experimental data is given in Table 5 along with the orifice Reynolds number. The values of d_{32} were seen to reduce when either increasing mass flow rate or reducing dispersed phase viscosity. Lower viscosity oils had log-normal distributions, higher viscosity oil distributions became skewed and then bimodal, with peaks at O(100 μm) and O(5 μm) respectively. It is interesting to note that the narrowest distributions occurs for the intermediate flow rates used.

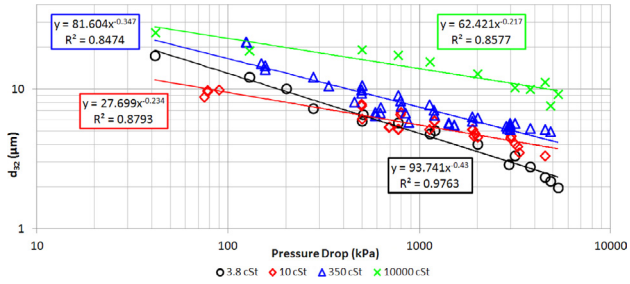

Fig. 5. Graph of d_{32} vs pressure drop for four different oil viscosities. SLES constant at 0.5 wt%, multiple orifices and experimental conditions included.

4.2. Influence of process parameters on drop size statistics

4.2.1. Effect of pressure drop

The data displayed in Fig. 5 show that as the pressure drop (which scales with flow rate) increased the measured d_{32} generally decreased with R^2 values all above 0.84 for all four oil viscosity series. The slopes of the correlation curves varied from −0.21 to −0.43 between different oil viscosities, with no clear trend seen as oil viscosity increased.

4.2.2. Effect of oil viscosity

Plots of d_{32} versus oil viscosity are given for orifice 0025 (Fig. 6a) and orifice 0080 (Fig. 6b), over a range of different mass flow rates. In each it is seen that as oil viscosity increased, droplet

Table 5
Values for d_{32} for different mass flow rates and oil viscosities. Oil at 10 wt% or less, SLES at 0.5 wt%, 0025 orifice.

Mass flow rate (kg·min^{-1})	Mass flow rate (kg·s^{-1})	Pressure drop (kPa)	*Re (orifice)*	d_{32} (μm) for DC245 (3.8 cSt)	d_{32} (μm) for 10 cSt silicone oil	d_{32} (μm) for 350 cSt silicone oil	d_{32} (μm) for 10,000 cSt silicone oil
2	0.033	503	29,300	5.24	6.08	11.17	24.75
3	0.050	1140	44,400	4.88	5.18	8.14	15.63
4	0.067	2022	59,500	4.21	4.66	6.59	12.20
5	0.083	3187	73,700	3.36	4.27	5.99	10.97
6	0.100	4598	88,700	2.42	3.01	5.15	9.63

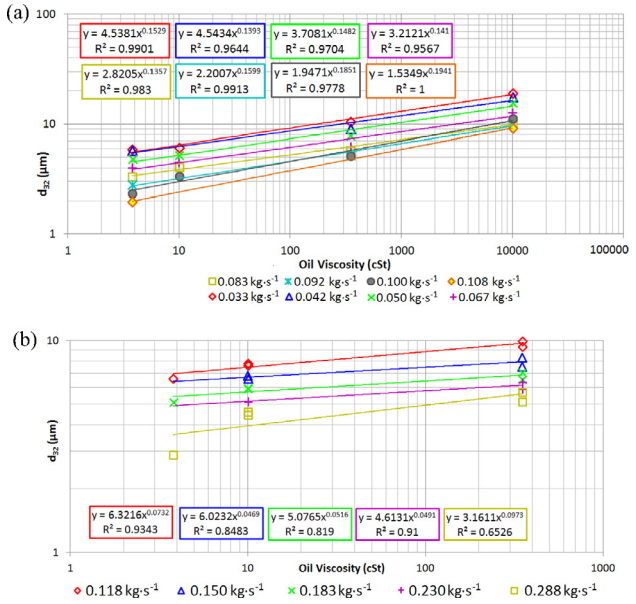

Fig. 6. Graphs of d_{32} vs oil viscosity. SLES constant at 0.5 wt%: (a) eight different mass flow rates using orifice 0025; (b) five different mass flow rates using orifice 0080.

size also increased. For the smaller orifice: coefficients of determination (R^2) were above 0.95, and slopes around 0.15. For the larger orifice: R^2 was above 0.81 for four out of five series, and slopes were between 0.046 and 0.098. It was clear at this stage, however, that oil viscosity affected the final droplet size significantly, but the effect was not as large as for pressure drop as evidenced by the lower slope magnitudes.

4.2.3. Effect of SLES concentration

The SLES concentration was varied from 0.5 wt% down to 0.0003 wt% using the 0080 orifice, and TMIX oil inlet condition, using 3.8 cSt and 350 cSt oils. In Fig. 7a (DC245) eight different data series for different flow rates are shown. The slope of trend lines was low and slightly negative: from 0.003 down to −0.063, with low scatter, as evidenced by generally high R^2 values.

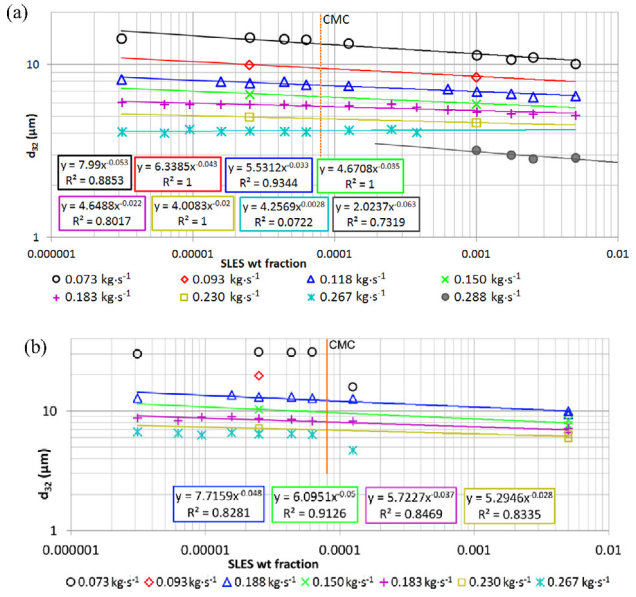

Fig. 7. Graph of d_{32} vs SLES weight fraction for orifice 0080: (a) 3.8 cSt oil (DC245) and eight mass flow rates; (b) 350 cSt oil and seven mass flow rates.

Different flow rates had different amounts of data; the biggest data set was obtained at a mass flow rate of 0.183 kg·s^{-1} with 15 different SLES concentrations, a slope of −0.022 and R^2 of over 0.8 is observed. Overall, for the 3.8 cSt oil there was a small but significant effect of SLES concentration on drop size.

In Fig. 7b the trends of d_{32} for varying SLES concentration for 350 cSt oil are shown. Only part of the SLES concentration range could be fully explored in the experimental time available. Power-law trendlines were fitted for the intermediate flow rates, with reasonably strong correlations except for two outliers. Poor correlation was observed for the highest and lowest flow rates, hence trendlines are not included here. Overall, there was a small but significant increase in droplet size as SLES concentration was lowered. The critical micelle concentration (CMC) for SLES is 0.008 wt%, shown on both graphs as a vertical orange line. Above the CMC, at equilibrium the interface should be saturated with surfactant, lowering interfacial tension; dynamic effects are not important due to the rapidity of the equilibration process (Hall et al., 2011). Below CMC this saturation might not occur, or occur more slowly, raising interfacial tension and possibly introducing Marangoni stresses due to interfacial tension gradients at the interface, depending on the competing timescales of interface formation and surfactant migration from the bulk to the interface. These phenomena might expect to cause deviations from linear behaviour, which are indeed observed for two data series for the 350 cSt oil in Fig. 7. However, this deviation could also be due to a shift from interfacial tension driven to viscosity driven droplet cohesive forces so these data do not enable these competing issues to be isolated. For the purposes of the present work, a straight line correlation is used, based on the majority of the data.

4.2.4. Effect of other variables

Some other variables which might have affected drop size were also investigated during the trials given in Table 2. Oil weight fraction was varied between 0.5 wt% and 10 wt%. Oil inlet condition was varied between PE, TMIX and INJ. Back pressure valve was usually in the open position, but some experiments were carried out with it in the closed position. None of these three variables were found to have a significant effect on droplet size; graphs of droplet size against these variables were flat on average, showing neither positive nor negative correlation.

Additionally, orifice size did not have any further effect on drop size except for its effect on influencing pressure drop over the Sonolator so these parameters are highly correlated. Also, multiple experimental rigs were used, and emulsification effects were found to be reproducible across these rigs.

5. Development of correlation for Sonolator droplet breakage data

A power law correlation was developed to predict d_{32} in terms of pressure drop, dispersed phase viscosity and SLES concentration. The power law indices were calculated by averaging the individual slopes for the lines of best fit (such as those in Figs. 5–7) for each variable, weighting these averages by the number of points in each data series. Some additional data not shown in the figures were also used in order to give maximum accuracy for the full range of experimental conditions, such as slopes of d_{32} vs pressure drop for SLES concentrations below 0.5 wt%. The final correlation produced is

$$\frac{d_{32}}{1\ \mu m} = 57.12\left(\frac{\Delta P}{1\ kPa}\right)^{-0.4061}\left(\frac{\nu_D}{1\ cSt}\right)^{0.1119} w_{SLES}^{-0.03846} \quad (7)$$

where ΔP is pressure drop is, ν_d is dispersed phase (oil) viscosity, and w_{SLES} is SLES weight fraction. Note that the first three of these

terms were dimensional; the correlation was non-dimensionalised by dividing the dimensional terms by the unit used in the calculations. This correlation was then compared to the original data in the graph below:

Predicted droplet size is compared to actual droplet size in Fig. 8. The data are found to cluster around the line of equality shown in orange. The spread of the data was elliptical around the line of best fit, indicating good agreement between predicted and actual values. This indicated that a single power law was appropriate to model droplet size for all viscosities. In particular, there was no significant difference in goodness of fit between the lower viscosity oils and the higher viscosity oils. The coefficient of determination (R^2) was 0.870 indicating reasonable predictive capability. Sources of scatter remaining were expected to include the smaller effects of the less significant variables, errors in experimental or sample analysis techniques, impurities in water or other materials used, inherent randomness in droplet breakage processes.

On the graph of d_{32} vs ΔP (Fig. 5) indices of dependence were −0.430, −0.234, −0.347 and −0.217 for viscosities 3.8 cSt, 10 cSt, 350 cSt and 10,000 cSt respectively; these gave some discrepancies from −0.4061, the index for ΔP in (7), and likewise small variations in slope were present for viscosity (Fig. 6) and SLES concentration (Fig. 7). In order to understand these differences, the data sets of individual slopes (from which the average slopes were constructed) were examined, this is given in full for pressure drop and summarised for viscosity and SLES concentration. In Fig. 9 the slopes for d_{32} vs pressure drop are plotted as a function of SLES weight fraction for four oil viscosities.

The slopes had a range of −0.62 to −0.22, with the majority of the data between −0.50 and −0.30. No consistent trend was seen either with viscosity or with SLES weight fraction. The reason why the indices for four viscosities separately had three out of four greater than −0.4061 (see Fig. 5) due to higher weightings of 0.5 wt % SLES data, with more data collected there and smaller slopes. Overall though, the slope of −0.4061 characterised the individual slopes in Fig. 9 well. A similar approach was taken for the slopes of d_{32} vs dispersed phase viscosity and slopes of d_{32} vs SLES weight fraction, the indices being respectively 0.1119 and −0.03846. These observations for pressure drop, viscosity and SLES concentration, taken together, provided the three indices for each component in the Sonolator power law correlation (7) above.

5.1. Comparison of theoretical and empirical drop size correlations

The empirical correlation developed is compared and contrasted with literature-based correlations in Table 6. Note: empirical indices of kinematic viscosity (ν_d) and dynamic viscosity (μ_d)

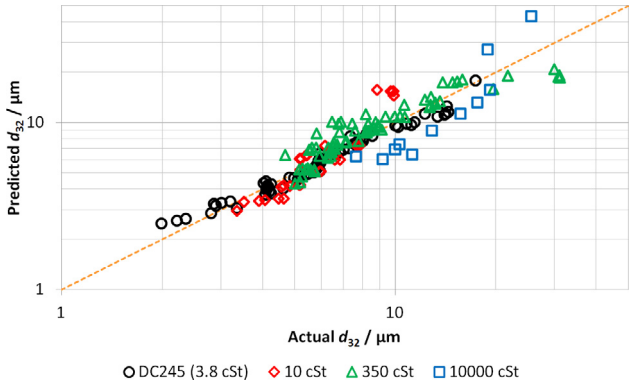

Fig. 8. Graph of predicted vs actual droplet sizes for different oil viscosities. Line in red is equality between predicted and actual. R^2 = 0.870.

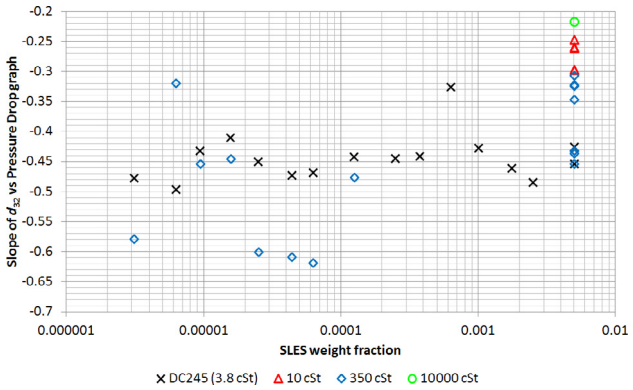

Fig. 9. Graph of slope (of d_{32} vs *pressure drop graph*) vs SLES weight fraction. Four different viscosity series illustrated.

were the same since the fluid in these experiments was always water, with constant density; these were used respectively in the Sonolator correlation (7) and in Table 6. Also, since pressure drop (ΔP) is approximately proportional to $\varepsilon^{2/3}$ (this is true by dimensional analysis when the length scale does not change by much, e.g. less than one order of magnitude across all pilot-scale Sonolators) the empirical result in Table 6 gave a droplet size proportionality of $\Delta P^{-0.4061}$.

The theoretical and experimental results (except Davies, 1987) were in the form of power laws. These were convenient because the effect of each term was independent, i.e. in the power law model ε had an independent effect on droplet size from the effect of viscosity. Power laws were also convenient since, when comparing them, it was only necessary to compare how the indices for the same variable changed. Comparing the indices for ε in Table 6, the value of −0.2707 was in the range of −0.4 to −0.25 for theoretical low and high viscosity TI break-up. This empirical index indicated that the regime was closer to high viscosity TI.

The dispersed phase viscosity (μ_d) indices in Table 6 were compared: the empirical index of 0.1119 was in the range of 0–0.75 for low and high viscosity TI break-up. It must be noted that Hinze (1955) used an assumption of inviscid flow, however his assumptions would also be true for low viscosity dispersed phase, where viscous forces $\ll$ interfacial forces. In that case, the index of dependence on the dispersed phase viscosity would be zero. This empirical index for viscosity indicated that the break-up regime was closer to low viscosity TI. Two other pieces of evidence were considered: firstly that between Fig. 4b and c (for 10 cSt, 350 cSt dispersed phase respectively) there the possibility for a change in droplet breakage mechanism; secondly, that in correlation (7) and its comparison to empirical data (Fig. 8) a single power law was found suitable to predict droplet sizes in both regimes, with no obvious "kink" indicating two different underlying regimes.

Hence the break-up mechanism observed in the Sonolator was within the bounds provided by low and high viscosity TI theories, however it did not consistently fit either model, nor seem to fit either model at different times under different working conditions. Instead, it appeared to occupy an intermediate regime. Walstra & Smulders (1998) stated that the droplet breakage regimes described in literature were idealised situations, and that intermediate regimes may occur in practice. Between low and high viscosity TI regimes, it is clear that in reality both interfacial tension and viscous resistance to deformation both occur simultaneously as cohesive forces acting on a droplet. Also, between TI and TV regimes a droplet not too much bigger than l_e might undergo both turbulent inertial break-up from small eddies, and some degree of turbulent viscous break-up from larger eddies which are all simultaneously present.

Table 6
Theoretical and empirical drop size correlations.

Author	Droplet size proportional to	Regime	Type	Pow(ε)	Pow(μ_d)
Hinze (1955)	$\varepsilon^{-0.4}\,\rho_c^{-0.6}\,\sigma^{0.6}$	TI (inviscid)	Theoretical	−0.4	0
Davies (1987)	$\varepsilon^{-0.4}\,\rho_c^{-0.6}\,\sigma^{0.6}\,(1+\beta\mu_d V'\sigma^{-1})^{0.6}$	TI (all)	Theoretical	Varies	Varies
Walstra and Smulders (1998)	$\varepsilon^{-0.25}\,\rho_c^{-0.75}\,\mu_d^{0.75}$	TI (high dispersed phase viscosity)	Theoretical	−0.25	0.75
Pilot plant data correlation	$\varepsilon^{-0.2707}\,\mu_d^{0.1119}\,w_{SLES}^{-0.03846}$	Sonolator	Empirical	−0.2707	0.1119

Other assumptions which were present in the idealised theories did not necessarily hold in Sonolator experiments. The theories assume that droplets break to equilibrium, since the theories had in mind systems such as batch stirred tanks where the conditions are held for hours at a time; however in the Sonolator the multiphase fluid traverses the Sonolator in a few tenths of a second, so breakage may well not continue to completion. Also it is assumed is that turbulence is isotropic: the Sonolator has a highly turbulent flattened jet in which all three components of turbulence, in terms of standard deviations of velocity in the three Cartesian directions, are different to each other. However, the theories in the literature only address the situation of isotropic turbulence due to the large mathematical simplifications in such an assumption. Further work is indicated in understanding non-isotropic systems from a theoretical standpoint. Given that the Sonolator data best fits the power law correlation given in (7), and that the pressure drop (or epsilon) index is intermediate between low and high viscosity TI theoretical values; examination of the indices for SLES concentration and viscosity remains.

Droplet size had a small dependence on surfactant (SLES) concentration, of empirical index −0.03846, for values of SLES weight fraction in the range 0.0003 wt% to 0.5 wt%. The CMC for SLES was estimated at 0.008 wt%, so the range of surfactant concentrations investigated was both above and below the CMC. From smallest to largest SLES concentrations was an increase in SLES concentration of 1600 times. The empirically estimated effect on droplet size of this increase in SLES concentration was therefore to change droplet size by a factor of $1600^{-0.03846} = 0.753$ times. Theoretically, interfacial tension should decrease from the oil-water value of 38 mN m^{-1} (quoted from Calabrese et al., 1986) to the oil-SLES-water value of around 11 mN m^{-1}, which is a factor of 0.2895 times. The interfacial tension index was 0.6 (for low-visc TI) or 0 (or hi-visc TI), hence droplet size should change by $0.2895^{0.6} = 0.475$ times to $0.2895^{0} = 1$ times (unchanged). Since $0.475 < 0.753 < 1$, the effect of surfactant concentration was in the range predicted by theory via the interfacial tension term.

However, measured interfacial tension of liquids at rest varies according to surfactant concentration not by a power law, but a sigmoidal curve with the largest effect of changing surfactant concentration around the order of magnitude of the CMC. However, in Fig. 7, for most data series a linear increase of d_{32} with SLES concentration was observed.

The theoretical models in the literature assume that interfacial tension is a constant. Dynamic interfacial tension effects caused by interface formation and deformation during droplet breakage, causing surfactant deplation and migration from the bulk are generally lacking in models in the literature. It is hoped that these results of power law dependency on surfactant concentration stimulate the development of new theoretical explanations.

Droplet size dependency upon dispersed phase viscosity (Fig. 6) was also a power law with fixed viscosity index of 0.1119 across a wide range of viscosities. This conflicted with the most accepted theoretical explanation by Davies (1987) in (4), which covers the whole of the TI regime, including intermediate viscosities, and predicts an effective viscosity index varying between 0 and 0.75. The experimental literature sometimes verified Davies' equation across all viscosities (Wang and Calabrese, 1986), sometimes verified it only for below 1000 cSt (Arai et al., 1977, Ludwig et al., 1997) and sometimes provided constant but different indices (0.7 (Pandolfe, 1981), 0.4 (Karbstein, 1994), 0.33 (Walstra and Smulders, 1998)).

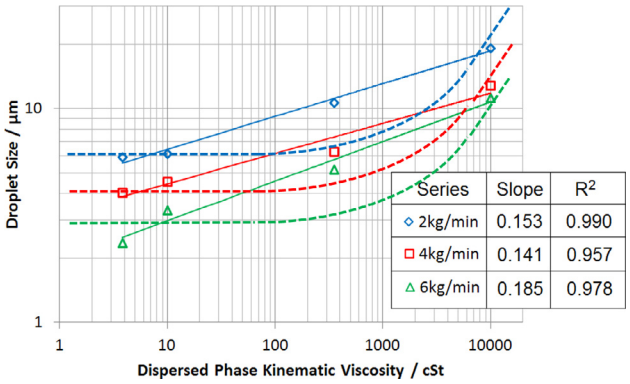

Fig. 10. Comparison of power law trends (solid lines) with Davies-type trends (dashed line).

Fig. 10 shows some of the Sonolator data from Fig. 6a along with power-law trend lines (solid) and trend lines as predicted by Davies (1987). There was no evidence in the data of a region of zero gradient, an intermediate slope and then a region of slope 0.75 as predicted by Davies. Hence although Davies' equation in (4) has been verified in the literature for some systems, it could not be verified for the Sonolator, which is why a fixed power-law index of 0.1119 was used instead; although this index was lower than other researchers' indices, it was clear from the data that higher fixed indices would not fit the data.

One possible explanation would be as follows: in the literature some of the drop size vs viscosity data series were flat at low viscosities, sharply upwards at around 100 cSt to 1000 cSt, and then flat thereafter (Arai et al., 1977, Ludwig et al., 1997). Such a curve would be possible to fit to the existing data, since there are measurements at only 4 different dispersed phase viscosities. Further work is therefore suggested to investigate the Sonolator with a more detailed set of dispersed phase viscosities, say with 10 different viscosities roughly equally spaced from 1 cSt to 10,000 cSt, and verify what the shape of the whole curve is; whether the fixed index model or the Davies' model is supported.

6. Conclusions

Emulsification in a pilot plant scale Sonolator has been characterised using silicone oil emulsions (with four different viscosities between 3.8 cSt and 10,000 cSt) in water with SLES as surfactant. Droplet size distributions (DSDs) have been obtained for this system for a variety of operating parameters using a laser scattering measuring technique. The most important statistic derived from each DSD was the average droplet size (d_{32}) and additionally the DSD shape could be summarised by the span (w) and skewness (s).

A power law correlation was developed to predict d_{32} based on input parameters. Flow rate through the Sonolator was an important input parameter which affected d_{32}. There were several

variables which were suitable to quantify flow rate, such as mass/volumetric flow rate, pressure drop and energy per unit mass; from these the pressure drop (ΔP) had the best correlation to d_{32} and was strongly correlated with orifice size. Dispersed phase viscosity (μ_d) was found to have a significant effect on d_{32}, whilst SLES concentration (w_{SLES}) had a minor effect. Some variables which did not have a significant effect on d_{32} included: back-pressure valve position, oil weight fraction (to 10 wt%), oil inlet condition (pre-emulsion, mixing at T-junction, injection), orifice size (when predicting d_{32} from pressure drop). The final correlation was a power law with indices of dependence −0.4061, 0.1119, −0.03846 for the three variables ΔP, μ_d, w_{SLES} respectively.

For fixed oil viscosity, given a specific pressure drop to create a specific droplet size, the distribution shape (span, skewness) was found to be constant, so it was not found possible to use other parameters to fine tune the droplet size distribution shape; this shape should be considered a characteristic of the Sonolator.

Emulsification in the Sonolator was found to take place in both low and high viscosity dispersed phase sub-regimes of the turbulent inertial (TI) droplet breakage regime. Three theoretical droplet size models were available from Hinze (1955), Davies (1987), and Walstra and Smulders (1998). The Sonolator empirical correlation was compared to these three droplet size models. The Sonolator correlation was found to be within the bounds of the theoretical models taken together, but did not fit neatly into any single model, in particular a regime change was not seen in the empirical data (Davies, 1987) but a single correlation fitted all empirical data. This indicated that intermediate droplet breakage regimes happen in practice, in between high and low viscosity breakage sub-regimes; this had also been supported by some experiments from the literature.

Acknowledgements

DJR was sponsored by the EPSRC Industrial Doctorate Centre in Formulation Engineering (EP/G036713/1) and Unilever Port Sunlight. The assistance of Steven Hall from University of Birmingham, and Adam Kowalski, Neil Adams, Kim Jones, John Naughton and Mark Flanagan from Unilever Port Sunlight with different aspects of the work are acknowledged. We also acknowledge Jumpstart UK (employer) for providing DJR with CPD time for writing papers and EngD thesis.

References

Arai, K., Konno, M., Matunaga, Y., Saito, S., 1977. Effect of dispersed-phase viscosity on the maximum stable drop size for breakup in turbulent flow. J. Chem. Eng. Jpn. 10, 325–330.

Baravian, C., Mougel, J., Caton, F., 2007. Characterization of Dynamical Emulsification Process in Concentrated Conditions. AIChE J. 53 (8), 1994–2000.

Calabrese, R.V., Chang, T.P.K., Dang, P.T., 1986. Drop breakup in turbulent stirred-tank contactors Part I: Effect of dispersed-phase viscosity. AIChE J. 32 (4), 657–666.

Calabrese, R.V., Francis, M.K., Mishra, V.P., Phongikaroon, S., 2000. Measurement and analysis of drop size in a batch rotor-stator mixer. In: van den Akker, H.E.A., Derksen, J.J., (Eds.), Proceedings of the 10th European Conference on Mixing, The Netherlands, July 2–5, 2000. Elsevier Science, Amsterdam, pp. 149–156.

Chen, H.T., Middleman, S., 1967. Drop size distribution in agitated liquid-liquid systems. AIChE J. 13 (5), 989–995.

Davies, J.T., 1985. Drop sizes of emulsions related to turbulent energy dissipation rates. Chem. Eng. Sci. 40 (5), 839–842.

Davies, J.T., 1987. A physical interpretation of drop sizes in homogenizers and agitated tanks, including the dispersion of viscous oils. Chem. Eng. Sci. 42 (7), 1671–1676.

El-Hamouz, A., 2007. Effect of surfactant concentration and operating temperature on the drop size distribution of silicon oil water dispersion. J. Dispersion Sci. Technol. 28 (5), 797–804.

Francis, M.K., 1999. The Development of a Novel Probe for the in situ Measurement of Particle Size Distributions, and Application to the Measurement of Drop Size in Rotor-Stator Mixers PhD Thesis. University of Maryland, College Park, MD, USA.

Hall, S., Cooke, M., El-Hamouz, A., Kowalski, A.J., 2011. Droplet break-up by in-line Silverson rotor–stator mixer. Chem. Eng. Sci. 66, 2068–2079.

Hall, S., 2012. Scale-up of Emulsification in Inline Rotor-Stator Mixers, EngD Thesis, University of Birmingham, UK.

Hall, S., Pacek, A.W., Kowalski, A.J., Cooke, M., Rothman, D., 2013. The effect of scale and interfacial tension on liquid-liquid dispersion in in-line Silverson rotor-stator mixers. Chem. Eng. Res. Des. 91 (11), 2156–2168.

Hinze, J.O., 1955. Fundamentals of the hydrodynamic mechanism of splitting in dispersion processes. AIChE. J. 1 (3), 295.

Karbstein, H., 1994. Ph.D. Thesis, University of Karlsruhe.

Koglin, B., Pawlowski, J., Schnoring, H., 1981. Kontinuierliches emulgieren mit rotor/statormaschinen: Einfluss der volumenbezogenen dispergierleistung und der verweilzeit auf die emulsionsfeinheit. Chem. Ing. Technol. 53 (8), 641–647.

Lin, C.Y., Chen, L.W., 2006. Emulsification characteristics of three- and two–phase emulsions prepared by the ultrasonic emulsification method. Fuel Process. Technol. 87, 309–317.

Ludwig, A., Flechtner, U., Pruss, J., Warnecke, H.-J., 1997. Formation of emulsions in a screw loop reactor. Chem. Eng. Technol. 20, 149–161.

Marmottant, P.H., Villermaux, E., 2004. Fragmentaion of stretched liquid ligaments. Phys. Fluids 16 (8), 2732–2741.

Padron, G.A., 2005. Effect of Surfactants on Drop Size Distribution in a Batch Rotor-Stator Mixer PhD Thesis. University of Maryland, College Park, MD, USA.

Pandolfe, W.D., 1981. Effect of dispersed and continuous phase viscosity on droplet size of emulsions generated by homogenization. J. Disp. Sci. Technol. 2, 459.

Puel, F., Briancon, S., Fessi, H., 2006. Chapter 6: Industrial technologies and scale-up. In: Benita, S., (Ed.), Microencapsulation: Methods and Industrial Applications, 2nd Ed., Drugs and the Pharmaceutical Sciences, Vol. 158. CRC Press Taylor & Francis Group, pp. 149–182.

Ryan, D., Simmons, M., Baker, M., 2017. Determination of the flow field inside a Sonolator liquid whistle using PIV and CFD. Chem. Eng. Sci. 163, 123–136.

Tesch, S., Freudig, B., Schubert, H., 2003. Production of emulsions in high-pressure homogenizers – Part I: Disruption and stabilization of droplets. Chem. Eng. Technol. 26 (5), 569–573.

Vankova, N., Tcholakova, S., Denkov, N.D., Ivanov, I.B., Vulchev, V.D., Danner, T., 2007. Emulsification in turbulent flow 1. Mean and maximum drop diameters in inertial and viscous regimes. J. Colloid Interface Sci. 312, 363–380.

Walstra, P., Smulders, P.E.A., 1998. Emulsion formation. In: Binks, B.P., (Ed.), Modern Aspects of Emulsion Science. The Royal Society of Chemistry, Cambridge, UK.

Wang, C.Y., Calabrese, R.V., 1986. Drop breakup in turbulent stirred-tank contactors part II: relative influence of viscosity and interfacial tension. AIChE J. 32 (4), 667–676.